Experimental Study, Dynamic Modelling, Validation and Analysis of Hydrogen Production from Biomass Pyrolysis/Gasification of Biomass in a Two-Stage Fixed Bed Reaction System

Akeem K. Olaleye[a], Kunle J. Adedayo[a], Chunfei Wu[b], Mohamad A. Nahil[b], Meihong Wang[a,*], Paul T. Williams[b,*]

[a] Process and Energy Systems Engineering Group, School of Engineering, University of Hull, Hull HU6 7RX, UK
[b] Energy Research Institute, The University of Leeds, Leeds, LS2 9JT, United Kingdom

ABSTRACT

There is great interest in producing hydrogen from renewable sources such as biomass rather than from fossil fuels. This paper presents new experimental results at different pyrolysis temperature and development of a dynamic model for a biomass pyrolysis/steam reforming process in a two stage fixed bed reactor. The model considers the hydrodynamics of the fixed bed reactor, the interfacial mass and energy transfer between the fluid-solid systems and the porous catalyst, and the energy transfer on a kinetic model. The 2D dynamic model resulted in a system of partial differential equations which was solved numerically in gPROMS®. The model was validated with the experimental results. The model predictions show good agreement with the experimental results. The model can be used as a useful tool for design, operation, optimization and control of the biomass steam gasification process.

Keywords: Biomass, Hydrogen production, Steam reforming, Gasification, Fixed bed reactor, Process Modelling

Nomenclature

Symbol	Description	Units
ΔH_i	Heat of reaction i	kJ/kg
C_j	Molar Concentration of component j	mol/ m^3
C_{pf}	Specific Heat Capacity of fluid	J/kg K
$D_{j,r}$	Diffusivity coefficient of component j in radial direction	m^2/s
$D_{j,z}$	Diffusivity coefficient of component j in axial direction	m^2/s
E_i	Activation energy of reaction i	kJ/mol
K_r	Thermal conductivity in radial direction	W/m K
K_z	Thermal conductivity in axial direction	W/m K
T_w	Temperature of wall	K
X_j	Conversion of component j	-
f_p	friction factor	-
k_i	rate constant of reaction i	
r_i	rate of reaction of reaction i	
u_j	superficial gas velocity	m/s
x_j	Mass fraction of component j	-
h	Heat transfer coefficient	W/ m^2 K
L	Length of reactor	m
N$_c$	Number of components	-
N$_r$	Number of reactions	-
N_j	Molar flux of component j	mol/s
p1-p5	Pyrolysis reactions	-
r1-r5	Reforming reactions	-

R	Radius of reactor	m
V	Volume	m^3
R_g	ideal gas constant	
$T(z,r)$	Temperature in the axial and radial direction	K
g	Gravitational constant	m/s^2
Q	Heat flow	J/s
Greek Symbol		
δ_{ij}	Order of reaction	-
α_{ij}	Stoichiometry of reaction	-
ε	Bed porosity	-
P	Density of component	kg/m^3
μ	Fluid viscosity	Pa. s

Subscript

s	Solid
b	bulk fluid
f	Fluid
w	Wall
wood	Wood
p	particle

1 Introduction

1.1 Background

Global energy demand is increasing with increase in world population and standard of living. Energy supply relies mainly on fossil fuels. With reserves of fossil fuels depleting and their use being the largest single source of greenhouse gas emissions, there is a shift towards the use of clean and renewable sources such as biomass fuels. Hydrogen has been identified as a clean and renewable source expected to play a significant role in future energy systems. The use of biomass pyrolysis and steam reforming for the production of hydrogen has drawn extensive interest from scientists, engineers and government agencies worldwide [1, 2]. Two-stage fixed bed reaction systems have been used extensively for investigating gasification processes due to advantages of easy temperature control at each stage, catalyst recycling and improved contacts between derived pyrolysis products and catalyst [3]. Current experimental practice is to construct fixed bed reactor for small scale research study. The fixed bed reactors are used repeatedly for experiments to predict product yields when new feedstock is used or when operating conditions change. With a model developed and validated using experimental results, the product yield can be predicted. Mathematical models of steam gasification can be used for studies of design, operation, and control of the reactors. This can avoid excessive experiments.

1.2 Literature Review

Hydrogen as a clean fuel has become attractive and its production from biomass has raise a lot of interest from researchers [4-7]. Enriched hydrogen gas can be produced from biomass via pyrolysis and steam reforming processes [4, 5]. Experimental studies have been carried

out using fixed bed reactors [1, 8-10], fluidized bed reactors [11], and screw kiln reactors [12].

Several studies through modelling and simulation have been carried out for fixed bed reactors. Ghavipour and Behbahani [13] developed a 1D unsteady state heterogeneous model to simulate adiabatic and non-adiabatic fixed-bed reactors for methanol to dimethyl ether reaction. Tinaut et al [4] presented a 1D steady state model of biomass gasification in a fixed bed downdraft gasifier. Di Blasi [9] presented a 1D unsteady mathematical model of fixed bed counter-current wood gasifiers. The model couples heat and mass transport with wood drying & devolatilization, char gasification, and combustion of both char and gas-phase species.

Several reaction models have been applied for pyrolysis and steam reforming of biomass. Hashimoto et al. [14] pointed out that several reaction kinetics models proposed for the pyrolysis of biomass have focused on estimating kinetic parameters. However, the kinetic parameters obtained from these experimental fitted models cannot be applied to any other biomass sample, as such new experiments will be necessary to estimate these parameters. Bamford et al. [15], Bilbao et al. [16], and Matsumoto et al. [17] modelled the pyrolysis of wood with a single first order reaction scheme but with fixed heat of reaction. Matsumoto et al modified the Bamford et al model by considering the oxidative rate of char removal. Grana et al. (2010) also proposed a two-stage reaction mechanism for the pyrolysis of biomass sample. Koufopanos et al. [18] proposed two competing and consecutive reactions accounting for both primary and secondary reactions.

1.3   Aim of this Study and its Novel Contribution

This paper presents experiments, dynamic modelling, model validation, and process analysis of biomass steam gasification. It offers a unique approach to predict the main product yields without the need for repeated experiments. New experimental results at different biomass pyrolysis temperature are presented for pyrolysis/steam reforming of wood sawdust. Previously, Wu et al. (2013a & 2013b) presented experimental results at fixed pyrolysis temperature (500 °C) for pyrolysis/steam reforming of biomass components using different catalysts. This study also developed a 2D dynamic model for biomass pyrolysis/steam reforming. Previous models for wood gasification have been based on steady state [4] and 1D dynamic model [9]. The model was validated and then used to carry out process analysis to predict product yields.

2   Experimental Setup/Procedures/Results

2.1   The Experimental setup

Several new experiments were carried out to investigate the influence of pyrolysis temperature on the hydrogen production from catalytic gasification of biomass. 1.0 g raw wood sawdust and 0.5 g 10 wt. % Ni/Al_2O_3 catalyst were used for each experiment, which was studied using a two-stage reaction system (a schematic diagram shown in Fig. 1). In each experiment, the second stage containing catalyst was heated up to 800 °C initially, then water was injected to the middle of the two reactors with a flow rate of 4.74 g/h, and the first reactor containing wood sawdust was heated to the designed temperature (300, 400, 500 or

600 °C) with a heating rate of 40 °C/min. The derived vapours from pyrolysis of wood sawdust pass through the catalyst bed in the presence of steam. The final products were condensed with two condensers in air atmosphere and dry ice respectively. Non-condensed gases collected in the Tedlar™ bag were analysed off-line by gas chromatography (GC). The total reaction time of each experiment was around 40 min, and N_2 with a flow rate of 80 mL/min was used as carrier gas.

H_2, CO and N_2 were analysed with a Varian 3380 GC on a 60-80 mesh molecular sieve column with argon carrier gas, whilst CO_2 was analysed by another Varian 3380 GC on a Hysep 80-100 mesh column with argon carrier gas. C_1 to C_4 hydrocarbons were analysed using a Varian 3380 gas chromatograph with a flame ionisation detector, with a 80-100 mesh Hysep column and nitrogen carrier gas.
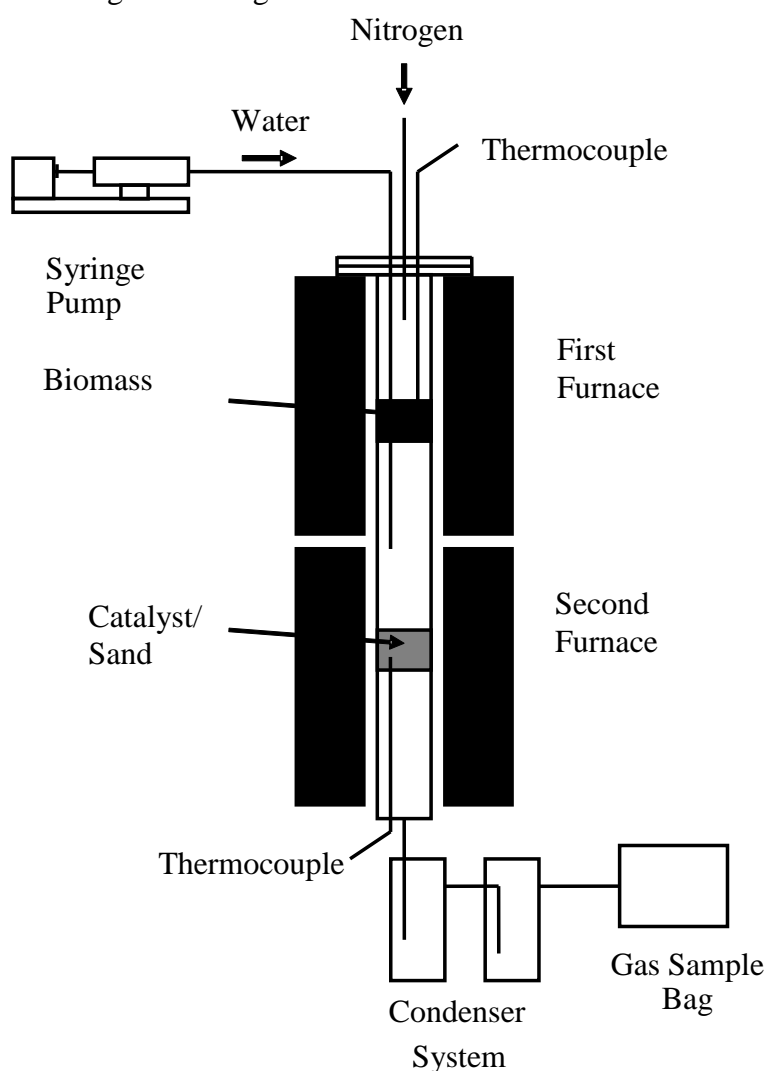

Figure 1: Schematic diagram of the pyrolysis/gasification of biomass

2.2   Experimental Results

The experimental results are shown in Table 1. It is shown that gas yield in terms of the weight of biomass was increased from 21.65 to 58.04 wt. % with the increase of pyrolysis temperature from 300 to 600 °C, while the char product (residue after pyrolysis) yield was reduced from 46.00 to 21.00 wt. %. In addition, the hydrogen yield calculated from the mole of produced hydrogen divided by the weight of raw biomass was increased significantly from

4.24 to 11.01 (mmol/g biomass). Product yield in terms of the weight of biomass and injected water were also presented in Table 1; the sum of gas, liquid, and char in relation to the total weight of biomass was close to 100 wt. % indicating good mass balance for the experiment.

Concentrations of non-condensed gases (N_2 free) are also shown in Table 1. The majority of gases from catalytic steam gasification of wood sawdust are H_2, CO and CO_2. Unlike the yield of products, gas concentration excluding carrier gas shows a different trend with the increase of pyrolysis temperature. It seems that H_2 concentration was reduced with the increase of pyrolysis temperature from 300 to 400 °C, and then H_2 concentration increased from 32.99 to 38.12 Vol.% with the further increase of pyrolysis temperature to 600 °C.

Table 1 Mass balance and gas concentration of biomass gasification at different pyrolysis temperatures

Pyrolysis temperature (°C)	300	400	500	600
Mass balance (wt. %)				
Gas/biomass	21.65	51.18	54.83	58.04
Char/biomass	46.00	28.00	25.00	21.00
Oil/biomass	32.35	20.82	20.17	20.96
H_2 yield (mmol/g biomass)	4.24	8.12	9.77	11.01
Gas concentration (Vol. %) (N_2 free)				
CO	25.16	29.67	31.74	29.51
H_2	40.04	32.99	36.49	38.12
CO_2	24.16	18.40	19.14	19.58
CH_4	8.60	13.71	9.56	9.85
C_2-C_4	2.04	5.22	3.07	2.94
Total	100.00	100.00	100.00	100.00

3   Dynamic Model Development and Validation

This section describes the dynamic model development of the two-stage fixed bed reactor for hydrogen production from pyrolysis/steam reforming of biomass.

3.1   *Model Assumptions*

To develop the 2D model of the two-stage fixed bed reactor the following conditions and assumptions [9, 19] were adopted: (a) conservation of mass and energy for the gas and the solid phase; (b) no momentum transfer; (c) the catalyst pellet is a porous solid with same pore size and shapes; (d) constant porosity of the bed; (e) constant thermal conductivity and diffusivity; (f) heat and mass transfer correlations for the non-reacting systems; (g) catalyst porosity included in the accumulation term *(it is assumed that accumulation only occurs in the gas phase)*.

3.2   *General Modelling Equations for the Fixed Bed Reactors*

The model consists of conservation equations for the solid and the gas phase fixed bed catalytic reactor, the catalyst particles as well as for the gas phase. The resistances to mass and heat transfer at the gas-solid interface were also considered.

For the mass balance equation, the diffusion and chemical reaction are important. Hence, the concentration of components j (i.e. C_j) vary with direction. This effect is particularly significant in the gas-phase species. Hence, the general mass balance equation (2-D) is developed as shown in Eq. (1) using the assumptions in section 3.1.

$$\varepsilon \frac{\partial C_j}{\partial t} = -\varepsilon u_z \frac{\partial C_j}{\partial z} + \varepsilon D_{j,z} \frac{\partial^2 C_j}{\partial z^2} + \varepsilon D_{j,r} \left(\frac{\partial^2 C_j}{\partial r^2} + \frac{1}{r} \frac{\partial C_j}{\partial r} \right) + \sum_{i \in reaction} \alpha_{i,j} r_i^* \qquad (1)$$

Where $\alpha_{i,j}$ is the stoichiometry of reaction i for component j and r_i^* is the rate of reaction i. Eq. (1) can be expressed in terms of mass fraction x_j thus;

$$\rho \frac{\partial x_j}{\partial t} = -\rho u_z \frac{\partial x_j}{\partial z} + \rho D_{j,z} \frac{\partial^2 x_j}{\partial z^2} + \rho D_{j,r} \left(\frac{\partial^2 x_j}{\partial r^2} + \frac{1}{r} \frac{\partial x_j}{\partial r} \right) + \sum_{i \in reaction} \alpha_{i,j} r_i^* \qquad (2)$$

where $D_{j,z}$ and $D_{j,r}$ are the axial and radial diffusivity respectively. The total mass fraction expected at the exit of the reactor should be equal to 1 i.e. $\sum_j x_j = 1$. The yield can be estimated thus;

$$yield = \frac{mass\ fraction\ of\ component\ j\ produced}{total\ mass\ fraction\ of\ the\ product}$$

$$yield(excluding\ inert) = \frac{mass\ fraction\ of\ component\ j\ produced}{total\ mass\ fraction - mass\ fraction\ of\ inert\ produced}$$

$$yield(excluding\ inert) = \frac{x_j}{1 - x_{inert}} \qquad (3)$$

The general energy balance for the fixed bed reactor is shown in Eq. (4)

$$\rho_f C_{pf} \varepsilon \frac{\partial T_b}{\partial t} = -\varepsilon \rho_f u_z C_{pf} \frac{\partial T_b}{\partial z} + \varepsilon K_z \frac{\partial^2 T_b}{\partial z^2} + \varepsilon K_r \left(\frac{\partial^2 T_b}{\partial r^2} + \frac{1}{r} \frac{\partial T_b}{\partial r} \right) + \Delta H_i \alpha_{i,j} r_i^* + Q \qquad (4)$$

Where T_b is the temperature of the bulk fluid, K_r and K_z are the thermal conductivities in the radial and axial direction respectively, ε is the porosity, C_{pf} is the heat capacity of the fluid, i for component j and r_i^* is the rate of reaction i.

3.3   Pyrolysis

In pyrolysis, organic materials (e.g. biomass) are converted or decomposed into volatile gases, bio-oil and char through a thermo-chemical process. It is necessary to develop model equations for pyrolysis of biomass to predict accurately the product yield [11].
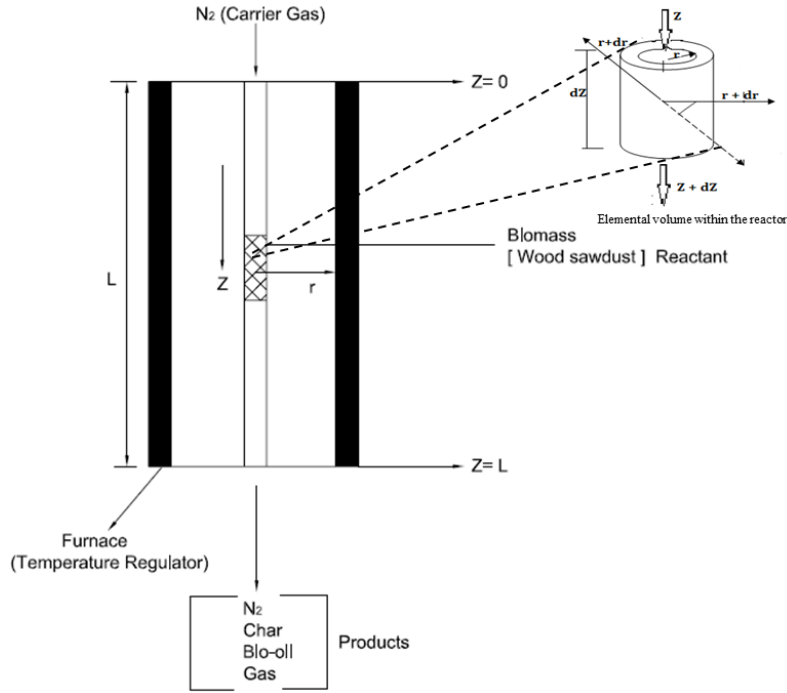
Figure 2: 1st stage Fixed bed Reactor for Biomass Pyrolysis

The effect of diffusion and convective flow was added into the mass balance over a differential volume of the fixed bed reactor (Figure 2). Eq. (2) and Eq. (4) in section 3.2 is the same for the 2-D mass and energy balance for the pyrolysis reactor. The rate of reaction r_i^* is expressed as

$$r_i^* = k_i \prod_{j=1}^{Nc} C_j^{\delta_{i,j}}, \quad k_i = k^* e^{-\frac{E_i(T)}{R_g T(z,r)}}$$

where k_i is the rate constant and its dependent on temperature in the axial and radial direction, $\delta_{i,j}$ is the reaction order for component j in reaction i. k^* is Arrhenius constant and E is the activation energy. Hence, the rate of reaction can be expressed thus

$$r_i^* = k^* \exp\left[\frac{E_i(T)}{R_g T}\left(\frac{1}{T_{in}} - \frac{1}{T(z,r)}\right)\right]\prod_{i=1}^{Nc}(C_j)^{\delta_{i,j}} \qquad (5)$$

The conversion X_j is

$$X_j = 1 - \frac{C_j}{C_{jO}} \qquad (6)$$

where C_{jO} represent the initial concentration of the fluid, X_j represents the conversion of reactant. The overall conversion at a given distance z from the reactor entrance is

$$X^*(z) = 1 - \frac{2\pi \int_0^R C_j u_z \, r dr}{F_{jo}} \qquad (7)$$

Initial and boundary conditions
1. for the radial concentration and temperature boundary conditions:

- No mass transfer to a boundary, at the wall of non-reacting pipe, no convective flow, hence, $C_j\big|_R = 0, \frac{\partial x_j}{\partial r} = 0$ at r = R
- At the tube wall r = R,
  heat $flux$ to the $wall$ $=$ $convective$ $flux$ out of the $reactor$
  $-K_r \frac{\partial T}{\partial r} = h(T - T_w)$ at r = R

- Concentration gradient of each specie for radial diffusion is zero at the centre of the reactor, $\frac{\partial x_{j,b}}{\partial r} = 0$, $\frac{\partial T}{\partial r} = 0$, at r = 0

2. for the axial concentration and temperature boundary conditions:
- At the entrance of the reactor, z = 0,

$$diffusive\ transfer = convective\ transfer$$

$$D_{j,z} \frac{\partial x_{j,b}}{\partial z} = u_z(x_{j,0} - x_{j,b})$$

- At the exit of the reactor z = L,

$\frac{\partial x_j}{\partial z} = 0$, $\frac{\partial T}{\partial z} = 0$, at z = L

3.3.1 Pyrolysis Reaction

Biomass materials are different according to the composition of their main components. Pyrolysis of biomass is significantly dependent on the main components of cellulose, hemicellulose and lignin [20]. During pyrolysis reaction, biomass materials (i.e. wood sawdust, grass, or rice husk) are decomposed to give gaseous compounds, bio-oil, and char due to temperature increase in the reactor. Wu et al [1] carry out experimental analysis of the properties of wood sawdust in terms of its ultimate and proximate analysis as shown in Table 2. The results of the new experiment described in section 2 will be used in this study for model validation.

Table 2: Proximate and Ultimate Analysis of the Wood Sawdust [1]

	Ultimate Analysis					Proximate Analysis			
	C	H	O	N	S	Moisture	Volatiles	Fixed Carbon	Ash
Wood sawdust	47.1	5.9	46.9	0. 1	0.02	6.4	74.8	18.3	1.2

Biomass pyrolysis involves a complex set of parallel and series chemical reactions influenced by heat and mass transfer. The selection of different reaction paths is based on the reaction mechanism adopted. In this study, we adopted the mechanism proposed by Chan [21] and presented in Sinha et al [22] for wood pyrolysis as shown in Figure 3. The wood sawdust was modelled as hydrocarbon ($CH_aO_bN_cS_d$) as shown in Table 3 using the elemental compositions in Table 2 and its molecular weight, neglecting the N and S components.

Table 3: Chemical Composition of Wood Sawdust

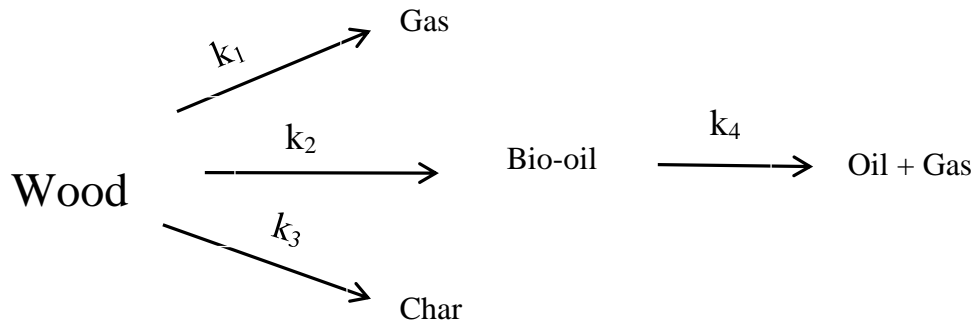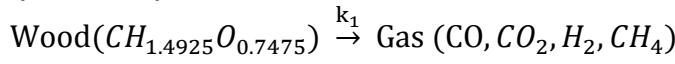| Coefficients (mol/mol C)	Parameters
a	1.4925
b	0.7475
c	0.0018
d	0.0002
Chemical Formula	$CH_{1.4925}O_{0.7475}$
Molecular weight (g/mol)*	99.79

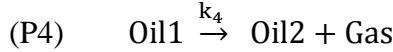* estimated from the chemical analysis in Table 2
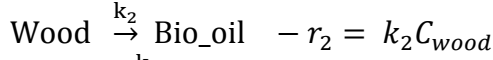
Figure 3: Pyrolysis of wood [21]

For wood sawdust;

P1. Gas formation from wood devolatilization:

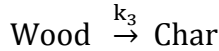$$\text{Wood}(CH_{1.4925}O_{0.7475}) \overset{k_1}{\to} \text{Gas } (CO, CO_2, H_2, CH_4)$$

reaction rate expression$: -r_1 = k_1 C_{Wood} \quad \Delta H_1 = 131 \frac{KJ}{mol}$

P2. Gas and Bio-oil formation: (consecutive reaction)

$$\text{Wood} \overset{k_2}{\to} \text{Bio\_oil} \quad -r_2 = k_2 C_{wood}$$

(P4) $\quad \text{Oil1} \overset{k_4}{\to} \text{Oil2} + \text{Gas}$

reaction rate expression: $-r_4 = k_4 C_{oil1} \quad \Delta H_2 = -74.8 \frac{KJ}{mol}$

P3. Char formation from Wood devolatilization:

$$\text{Wood} \overset{k_3}{\to} \text{Char}$$

reaction rate expression: $-r_3 = k_3 C_{wood} \quad \Delta H_3 = 172 \frac{KJ}{mol}$

3.3.2 Model Equations for the Pyrolysis reactions

Fluid Phase

Gas and Oil component balance in the reactor: The general equation remains the same, due to the nature of diffusivity or convective flow of their molecules

$$\rho \frac{\partial x_j}{\partial t} + \rho u_z \frac{\partial x_j}{\partial z} = \rho D_{j,z} \frac{\partial^2 x_j}{\partial z^2} + \rho D_{j,r} \left(\frac{\partial^2 x_j}{\partial r^2} + \frac{1}{r} \frac{\partial x_j}{\partial r} \right) + \sum_{i,j} \alpha_{i,j} r_i \qquad (8a)$$

or expressed in mass concentration,

$$\frac{\partial \rho_j}{\partial t} + u_z \frac{\partial \rho_j}{\partial z} = D_{j,z} \frac{\partial^2 \rho_j}{\partial z^2} + D_{j,r} \left(\frac{\partial^2 \rho_j}{\partial r^2} + \frac{1}{r} \frac{\partial \rho_j}{\partial r} \right) + \sum_{i,j} \alpha_{i,j} r_i \qquad (8b)$$

Energy balance:

$$\rho_f C_{pf} \varepsilon \frac{\partial T_b}{\partial t} = -u_z \rho_f C_{pf} \varepsilon \frac{\partial T_b}{\partial z} + \varepsilon K_z \frac{\partial^2 T_b}{\partial z^2} + \varepsilon K_r \left(\frac{\partial^2 T_b}{\partial r^2} + \frac{1}{r} \frac{\partial T_b}{\partial r} \right) + \Delta H_i \alpha_{i,j} r_i^* + Q \quad (9)$$

Solid Phase

Char: the equation is reduced and simplified since char is solid (negligible diffusion),

$$q \frac{\partial x_j}{\partial t} + \rho u_z \frac{\partial x_j}{\partial z} = \sum_{i,j} \alpha_{i,j} r_i \qquad (10a)$$

or

$$\frac{\partial \rho_j}{\partial t} + u_z \frac{\partial \rho_j}{\partial z} = \sum_{i,j} \alpha_{i,j} r_i \qquad (10b)$$

Char energy balance:

$$\rho_f C_{pf} \varepsilon \frac{\partial T_b}{\partial t} = -\varepsilon u_z \rho_f C_{pf} \frac{\partial T_b}{\partial z} + \Delta H_i \alpha_{i,j} r_i^* + Q \qquad (11)$$

Wood: wood is solid and cannot diffuse but possesses convective fluid-like properties

$$\rho \frac{\partial x_j}{\partial t} = \sum_{i,j} \alpha_{i,j} r_i \qquad (12)$$

Wood energy balance:

$$\rho_f C_{pf} \varepsilon \frac{\partial T_b}{\partial t} = \varepsilon K_{j,z} \frac{\partial^2 T_b}{\partial z^2} + \Delta H_i \alpha_{i,j} r_i^* + Q \qquad (13)$$

Where,

$$r_i = k^* e^{-\frac{E_i(T)}{R_g T(z,r)}} \prod_{i=1}^{N_c} (x_j)^{\delta_{i,j}} \qquad (14)$$

Where j = wood, gas, oil, and char in equations (8) – (14). For $k_1 \gg k_2 \; and \; k_3$ more gas is formed. Also, with an increase in the temperature of the reactor, the forward reaction is favoured. Oil and Char undergo thermal cracking to produce more gas at high temperature. The kinetic parameters for the pyrolysis were obtained from literature as shown in Table 4. The kinetic parameter for the secondary cracking of bio-oil was obtained from Boronson [23].

Table 4: Kinetic Constants for the pyrolysis reactions

Rxn	Wood (s^{-1})		Wood (Estimated)*
p1	$1.3 \times 10^8 \, e^{-\frac{16839}{T}}$	[21]	$4.7 \times 10^8 \, e^{-\frac{18745}{T}}$
p2	$2 \times 10^8 e^{-\frac{15997}{T}}$	[21]	$1.5 \times 10^9 e^{-\frac{17045}{T}}$
p3	$1.08 \times 10^7 \, e^{-\frac{14554}{T}}$	[21]	$3.41 \times 10^7 \, e^{-\frac{12884}{T}}$
p4	$1.48 \times 10^6 \, e^{-\frac{17320}{T}}$	[23]	$2.72 \times 10^6 \, e^{-\frac{19451}{T}}$

* Obtained using gPROMS Parameter estimation capabilities

3.4   Steam Reforming

Steam reforming is a thermo-chemical process involving the partial combustion of organic materials in a flowing gas with minimal oxygen at a temperature higher than fast pyrolysis. The steam reforming occurs in the second stage fixed bed reactor (Figure 4) resulting in gas products. The heat transfer to the product in the second stage is achieved by entraining products from the pyrolysis reactor into a fresh steam which is then passed through an externally heated tubular reactor. In order to improve the process performance the use of catalysts has also been proposed [1, 10, 24]. The operation requires high operating temperatures and very short contact times.
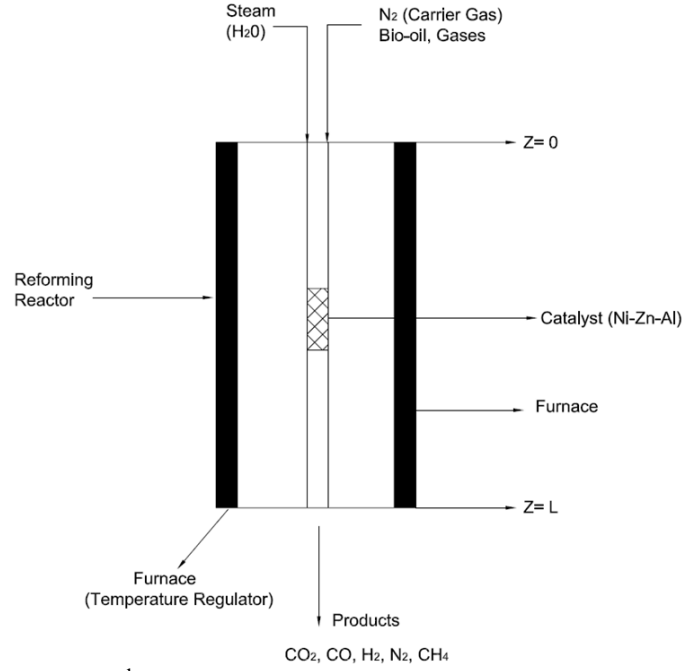
Figure 4: 2nd Stage Fixed Bed reactor for Steam Reforming

Figure 4: 2$^{\text{nd}}$ Stage Fixed Bed reactor for Steam Reforming

3.4.1 Mutual Balance on the Steam Reforming Reactor

Expressing the laws of conservation of mass in terms of mass concentration in axial (z-direction), we have

$$\frac{\partial(u_i\rho_j)}{\partial z} + \frac{\partial(\rho_j)}{\partial t} + \frac{\partial(N_j)}{\partial z} - \alpha_{i,j}r_j = 0 \tag{15}$$

Similarly, for radial (r-direction)

$$\frac{\partial(u_i\rho_j)}{\partial r} + \frac{\partial(\rho_j)}{\partial t} + \frac{\partial(N_j)}{\partial r} - \alpha_{i,j}r_j = 0 \tag{16}$$

For component *A* in a bulk and incompressible fluid in both directions, we thus have

$$\nabla.u\rho_j + u.\nabla N_j + \frac{\partial\rho_j}{\partial t} - \alpha_{i,j}r_j = 0 \tag{17}$$

Where the flux N_j can be expressed in terms of mass concentration, $\alpha_{i,j}$ is the reaction stoichiometry coefficient of component *j*, in reaction *i*. From Fick's law of diffusion, for axial direction,

$$N_{j|z} = -D_{j,b}\frac{\partial\rho_j}{\partial z} \tag{18}$$

for both direction,

$$N_j = -D_{j,b}\nabla\rho_j \tag{19}$$

For a constant diffusivity flux, $D_{j,b}$

$$\nabla.u\rho_j + \frac{\partial\rho_j}{\partial t} = D_{j,b}\nabla^2\rho_j + \sum_{i,j}\alpha_{i,j}r_j \tag{20}$$

We can then transform the above equation to

$$\rho_j\nabla.u + \frac{D\rho_j}{Dt} = D_{j,b}\nabla^2\rho_j + \sum_{i,j}\alpha_{i,j}r_j \tag{21}$$

Hence, for a multicomponent fluid system with constant fluid velocity along axial direction and negligible fluid velocity along radial direction, we have

$$\frac{\partial\rho_j}{\partial t} + u_z\frac{\partial\rho_j}{\partial z} = D_{j,z}\frac{\partial^2\rho_j}{\partial z^2} + D_{j,r}\left(\frac{\partial^2\rho_j}{\partial r^2} + \frac{1}{r}\frac{\partial\rho_j}{\partial r}\right) + \sum_{i,j}\alpha_{i,j}r_i \tag{22}$$

Energy balance on the steam reforming reactor

The energy balance around the reforming reactor is;

$$\rho_f C_{pf} \varepsilon \frac{\partial T_b}{\partial t} = -\varepsilon \rho_f u_z C_{pf} \frac{\partial T_b}{\partial z} + \varepsilon K_{j,z} \frac{\partial^2 T_b}{\partial z^2} + \varepsilon K_{j,r} \left(\frac{\partial^2 T_b}{\partial r^2} + \frac{1}{r} \frac{\partial T_b}{\partial r} \right) + \Delta H_i \alpha_{i,j} r_i^* + Q \quad (23)$$

Initial and Boundary Conditions

Radial:

- $N_j|_R = 0$, $\quad \frac{dC_{j,b}}{dr} = 0 \quad at \ r = R$
- Planes of symmetry. $\frac{dC_{j,b}}{dr} = 0 \quad at \ r = 0$

Axial:

- At the entrance of the reactor $z = 0$,

$diffusive \ transfer = convective \ tranfer$

$$D_{j,z} \frac{\partial C_{j,b}}{\partial z} = u_j \left(C_{j,0} - C_{j,b} \right) \quad at \ z = 0$$
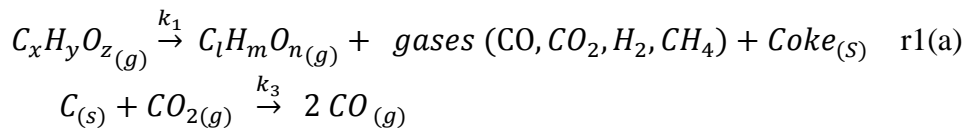
- at the exit of the reactor $z = L$

$$\frac{dC_j}{dz} = 0 \quad at \ z = L$$

3.4.1 Steam Reforming Reactions

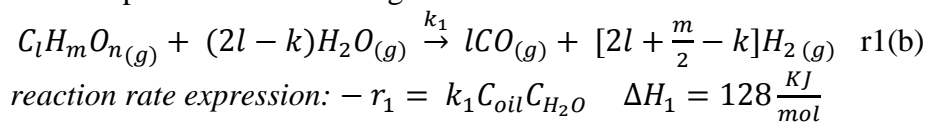The steam reforming reactions include the reactions of bio-oil (modelled as $CH_{1.522}O_{0.0228}$ according to Bryden and Ragland [25] with molar mass of 94 g/mol [26]) and the non-condensable gases (CO, CH_4, CO_2, H_2 etc.) with steam to H_2 and CO_2. The gas is mixed with steam and preheated before it is channelled into the reformer. This consists of reactor pipes containing a nickel catalyst. In this way, the gas–steam mix is transformed to H_2, CO, CO_2 and water. Considerable excess steam is used in the process. The synthesis gas exits the reformer and enters a shift converter. The carbon monoxide contained in the gas is then converted into H_2 and CO_2 using steam.
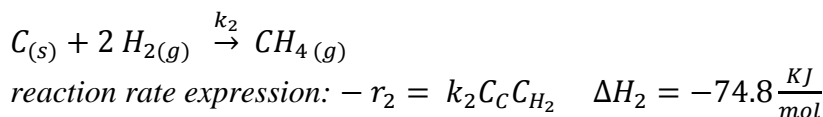
r1. Bio-oil (tar) steam reforming reaction

Steam reforming of bio-oil presents significant difficulties, especially in terms of carbonaceous deposits (i.e. coke formation). Due to the high temperature of the reaction, it is likely that partial thermal decomposition (r1(a)) and the Boudouard reaction (r3) can occur simultaneously [27]:
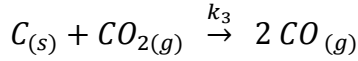
$$C_x H_y O_{z(g)} \overset{k_1}{\rightarrow} C_l H_m O_{n(g)} + \ gases \ (CO, CO_2, H_2, CH_4) + Coke_{(S)} \quad r1(a)$$

$$C_{(s)} + CO_{2(g)} \overset{k_3}{\rightarrow} 2 \ CO_{(g)}$$

The complete steam reforming reaction of bio-oil is

$$C_l H_m O_{n(g)} + (2l - k)H_2 O_{(g)} \overset{k_1}{\rightarrow} lCO_{(g)} + [2l + \frac{m}{2} - k]H_{2 \ (g)} \quad r1(b)$$

reaction rate expression: $- r_1 = \ k_1 C_{oil} C_{H_2 O} \quad \Delta H_1 = 128 \frac{KJ}{mol}$

r2. Methanation reaction

$$C_{(s)} + 2 \ H_{2(g)} \overset{k_2}{\rightarrow} CH_{4 \ (g)}$$

reaction rate expression: $- r_2 = \ k_2 C_C C_{H_2} \quad \Delta H_2 = -74.8 \frac{KJ}{mol}$

r3. Boudouard reaction

$$C_{(s)} + CO_{2(g)} \xrightarrow{k_3} 2\,CO_{(g)}$$
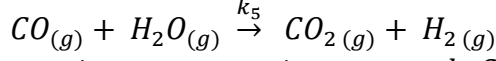
reaction rate expression: $-r_3 = k_3 C_C C_{CO_2}$ $\Delta H_3 = 172\,\frac{KJ}{mol}$

r4. Methane steaming reforming reaction

$$CH_{4\,(g)} + H_2O_{(g)} \xrightarrow{k_4} CO_{(g)} + 3\,H_{2\,(g)}$$
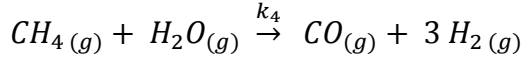
reaction rate expression: $-r_4 = k_4 C_{CH_4} C_{H_2O}$ $\Delta H_4 = 206\,\frac{KJ}{mol}$

r5. Water gas shift reaction

$$CO_{(g)} + H_2O_{(g)} \xrightarrow{k_5} CO_{2\,(g)} + H_{2\,(g)}$$

reaction rate expression: $-r_5 = k_5 C_{CO} C_{H_2O}$ $\Delta H_5 = -41\,KJ/mol$

Table 5: Kinetic Parameter for the steam reforming reactions

Reaction	Literature Values	References	This model (Estimated*)
r1	$3.12 \times 10^{-2}\, e^{-\frac{530.4}{T}}$	[28]	$2.27 \times 10^{-1}\, e^{-\frac{551.8}{T}}$
r2	$0.12\, e^{-\frac{17921}{T}}$	[5]	$1.0\, e^{-\frac{18051}{T}}$
r3	$4.40\, e^{-\frac{1.62x\,10^8}{T}}$	[5]	$4.81\, e^{-\frac{1.71x\,10^8}{T}}$
r4	$3.0 \times 10^5\, e^{-\frac{15000}{T}}$	[5]	$4.5 \times 10^5\, e^{-\frac{14800}{T}}$
r5	$10.20\, e^{-\frac{44.5}{T}}$	[5]	$17.57\, e^{-\frac{53.83}{T}}$

* Obtained using gPROMS Parameter estimation capabilities

3.5   Catalyst Particle

3.5.1 Catalyst/Gas Interface Flow Modelling

Although the catalyst particles of a fixed bed may not be spherical, an analysis based on flow in a regularly packed bed of spheres gives good approximation for heat transfer. The spheres are assumed to be packed in the closest possible arrangement. The bed consists of parallel layers of spheres in planes normal to the direction of flow. The method of assumption is that for any sphere in the bed, the heat transfer is the same as it would be for flow past a single sphere at the velocity through one of the orifices between the spheres.

The centre of the sphere is chosen as the origin of the coordinate system. At radial distance *r* from the centre, we have a spherical surface at a uniform temperature *T*. At distance *r+dr* is another surface at temperature *T+dT*. These two surfaces can be considered as the boundaries of the control volume.

Hence,

$$volume\ of\ sphere\ (V) = 4\pi r^2 dr \qquad (24)$$

$$Rate\ of\ heatflow\ into\ control\ volume\ =\ -K(4\pi r^2)\frac{\partial T_p}{\partial r_p} \quad (25)$$

$$Rate\ of\ heatflow\ out\ of\ control\ volume\ =\ -K(4\pi(r+dr)^2)\left[\frac{\partial T_p}{\partial r_p}+d\frac{\partial T_p}{\partial r_p}\right] \quad (26)$$

$$input-output=accumulation$$

The Net heat flow can be found by subtracting (25) from (26).

$$Net\ heat\ flow\ =\ 4\pi K(r^2\frac{\partial^2 T_p}{\partial r_p^2}dr+2r\frac{\partial T_p}{\partial r_p}dr) \quad (27)$$

$$accumulation\ of\ energy\ =\ (4\pi r^2 dr)\rho Cp\frac{\partial T_p}{\partial \theta} \quad (28)$$

Substituting both accumulation and net flow in into the balance and introducing the reaction term therefore we have

$$(4\pi r^2 dr)\rho Cp\frac{\partial T_p}{\partial \theta}\ =\ 4\pi K(r^2\frac{\partial^2 T_p}{\partial r_p^2}dr+2r\frac{\partial T_p}{\partial r_p}dr)+\sum_j -\Delta H_j r_{j,s}^* \quad (29)$$

Dividing equation (29) by $4\pi r^2 dr$, from which we obtain the equation for unsteady state conduction

Energy balance:

$$\rho_s C_{ps}\varepsilon_s\frac{\partial T_s}{\partial t}\ =\ \varepsilon_s K_{i,s}\left(\frac{\partial^2 T_s}{\partial r_s^2}+\frac{2}{r_s}\frac{\partial T_p}{\partial r_s}\right)+\sum_j -\Delta H_j r_{j,s}^* \quad (30)$$

Similarly for mass balance on specie i:

$$\varepsilon_s\frac{\partial C_{i,s}}{\partial t}\ =\ \varepsilon_s D_{i,s}\left(\frac{\partial^2 C_{i,s}}{\partial r_s^2}+\frac{2}{r_s}\frac{\partial C_{i,s}}{\partial r_s}\right)+\sum_j \alpha_j r_{j,s}^* \quad (31)$$

Initial and Boundary Conditions

$at\ t=0$;

Concentration: $C_{i,s}=\ C_{i,0}$;

Temperature: $T_s=\ T_0$;

Boundary conditions:

at reactor centre $r=0$ and at all time ; $z\in(0,L)$;

concentration: $\qquad\qquad\qquad\qquad\frac{\partial C_{i,s}}{\partial r_s}|_{r_s=0}=\ 0$

Temperature: $\qquad\qquad\qquad\qquad\frac{\partial T_s}{\partial r_s}|_{r_s=0}=\ 0$

at reactor perimeter $r=R$ and at all time ; $z\in(0,L)$;

concentration: $\qquad C_{i,s}=\ C_{i,c}$

Temperature: $\qquad T_s=\ T_c$

3.5.2 Heterogeneous Catalysis Reaction

Volatile species in the reactor may further be broken down into smaller gases within the particles during transport either heterogeneously by reaction with the char or solid biomass, or homogeneously in the gas phase [23]. The complexity in the reaction system makes it extremely difficult to model reactions of individual components involved in pyrolysis; however, simplified models have been proposed using lumped products such as gases, oil and char and could provide good insight to the overall process [23].

Applying the Langmuir-Hinshelwood reaction mechanism to the secondary cracking of oil, where A (oil), and B (gas product formed) are the reactant and product respectively.

1. $\qquad A_{(g)}+S\ \xrightarrow{k_1,\,k_2}\ AS$

2. $\qquad AS\ \xrightarrow{k_3}\ BS\quad$ *rate determining step*

3. $\qquad BS\ \xrightarrow{k_4,\,k_5}\ B_{(g)}+S$

From reaction (1) the rate of the reversible reaction with respect to the forward and the backward reaction is given by

$$-r_1 = k_1 C_A C_S - k_2 C_{AS} \qquad (32)$$

From reaction (3), since reaction (2) is the rate determining step,

$$-r_3 = k_5 C_B - k_4 C_B C_S \qquad (33)$$

For steady state approximation, $-r_1 = -r_3 = 0$

Hence reaction (1) becomes: $C_{AS} = \dfrac{k_1 C_A C_S}{k_2}$ and reaction (3) $C_{BS} = \dfrac{k_5 C_B C_S}{k_4}$

From reaction (2), $-r_2 = k_3 C_{AS}$, substituting for AS in the above equation;

$$-r_2 = k_3 \left(\frac{k_1 C_A C_S}{k_2}\right)$$

The total concentration of active sites $= 1$

Therefore: $C_{AS} + C_S + C_{BS} = 1$

Substituting for AS, BS in the above equation

$$\frac{k_1 C_A C_S}{k_2} + \frac{k_5 C_B C_S}{k_4} + C_S = 1$$

$$C_S = \frac{1}{1 + K_1 C_A + K_4 C_B}$$

Substituting for C_S in the above equations

$$-r_2 = k_3 \left(\frac{k_1 C_A}{k_2}\right)\left(\frac{1}{1 + K_1 C_A + K_4 C_B}\right) \qquad (34)$$

$$rate\ of\ reaction\ (r_i^*) = k^* e^{-\frac{E}{RT(z,r)}} \prod_{j=1}^{N_c} C_j{}^{\delta_{i,j}} \qquad (35)$$

3.6 Hydrodynamics of the Fixed Bed

Flow of a fluid through a packed bed or granular particles occurs frequently in chemical processes i.e. fixed bed reactor. As for flow past tube banks, there exist many correlations for calculating the pressure drop in flow through a fixed bed. We choose to apply the method based on the use of *Hydraulic radius (r_H)*. This method is applicable to incompressible beds composed of nearly spherical particles. The bed porosities (fractional void-space) may range from 0.3 - 0.6. A successful method for the prediction of the behaviour of flow through a bed from flow past a single sphere is given by Ranz and Marshall [29].

For the fixed bed with N_p particles,

$$r_H = \frac{void\ volume\ of\ bed}{surface\ area\ of\ packing} \qquad (36)$$

If the V_p represents the volume of particles and S_p represents the surface area of a particle, then the specific surface of a particle is defined by

$$S_v = \frac{S_p}{V_p} \qquad (37)$$

For spherical particle: $\quad S_v = \dfrac{6}{d_p} \qquad (38)$

$$\varepsilon = \frac{void\ volume}{volume\ of\ bed}, \quad \varepsilon = \frac{\rho_c - \rho_B}{\rho_c} \qquad (39)$$

Reynolds number: $R_{ep} = \dfrac{d_p u_{bs} \rho_g}{\mu(1-\varepsilon)} \qquad (40)$

Friction factor, $f_p = \dfrac{150}{R_{ep}} + 1.75 \qquad (41)$

Hence, pressure drop across bed is calculated thus;

$$-\Delta P = \frac{f_p L u_{bs}{}^2 (1-\varepsilon)\rho_g}{gD\varepsilon^3} \qquad (42)$$

There are few systems, however in which mass transfer occurs between a solid and a fluid and in such systems we have not only laminar boundary layer adjacent to the solid surface, but also the possibility of developed laminar flow throughout the fluid phase

Velocity profile for the plug flow:

$$u_z = u_0$$

For laminar flow, the velocity profile is

$$u_z = 2u_0 \left[1 - (\frac{r}{R})^2\right] \qquad (43)$$

Where u_0 is the average velocity inside the reactor and R is the fixed bed reactor radius.

Table 6 Parameters for Fixed Bed Properties for Wood

Parameters	Value	Reference
ρ_w	360.0 kg/m^3	[9]
ε	0.3	[9]
L	2.0 m	[1]
R	0.5 m	[1]
d_p	0.002 m	[1]
g	9.81 m/s^2	
$T_w = T_s = T_{in}$	300 K	
h	1.256 W/m^2 K	[9]

3.7 Parameter Estimation

Optimization technique is used in parameter estimation where sum of squared errors between the experimental and estimated values is minimized [30]. The parameter estimation entity in gPROMS® was used to estimate the kinetic parameters of the model. The literature values of the kinetic parameters were supplied as the guess value. This activity was carried out for both the pyrolysis and the steam reforming stages. Table 4 and Table 5 show the literature and estimated parameters used in this model for both pyrolysis and steam reforming stages respectively.

3.8 Numerical Solution of the model

The dynamic model results in a set of partial differential and algebraic equations (PDAEs) describing the mass and energy balances. The resulting PDAEs were solved by the SRADAU solver in gPROMS. The axial and the radial variables were discretized using the method of centred finite differences and orthogonal collocation respectively on finite elements over a uniform grid. All the simulations were performed at a time step of 0.01s and spatial steps of 0.1 cm. The solver MXLKHD, specifically designed for solving maximal likelihood optimisation problems is used for Parameter estimation in gPROMS®. This solver applies a sophisticated sequential quadratic programming (SQP) method to find the global optimum.

4   Model Validation

Steady-state performance of the model was validated using experimental data in Section 2. The two-stage reaction system is a fixed bed reactor with a diameter of 0.2 m and a total height of 2.0 m. Table 6 shows the summary of the parameters for the bed properties of the wood sawdust used for the experiment. Simulation results were validated using the product yield of the two-stage fixed bed reactor in the experiment as shown in Table 1. In addition, the measured gas concentration (vol. %, N_2 free) taken at different reforming temperature was compared with values obtained from the model. Table 7 to Table 11 shows the comparison of the experimental results and the model prediction.

Table 7 Validation of Char yield at outlet of pyrolysis reactor

Temperature (^{o}C)	Experiment (wt. %)	Model (wt. %)	Relative Error (%)
300	46	45.61	0.85
400	28	26.64	4.86
500	25	23.96	4.16
600	21	20.69	1.48

Table 8 Validation of Oil yield at outlet of pyrolysis reactor

Temperature (^{o}C)	Experiment (wt. %)	Model (wt. %)	Relative error (%)
300	32.35	31.05	4.02
400	20.82	21.05	1.10
500	20.17	20.87	3.47
600	20.96	20.78	0.86

Table 9 Validation of Gas yield at outlet of pyrolysis reactor

Temperature (^{o}C)	Experiment (wt. %)	Model (wt. %)	Relative error (%)
300	21.65	23.34	7.81
400	51.18	52.31	2.21
500	54.83	55.17	0.62
600	58.04	58.53	0.84

Table 10 Validation of Hydrogen yield at reformer outlet

Temperature (^{o}C)	Experiment (mmol/g)	Model (mmol/g)	Relative error (%)
300	4.24	4.43	4.48
400	8.12	8.51	4.80
500	9.77	10.04	2.76
600	11.01	11.17	1.45

Table 11 Validation of Gas Composition (vol. %) at reformer outlet

Temperature (°C)	Components List	Experiment (vol. %)	Model (vol. %)	Relative error (%)
300	CO	25.16	25.60	1.74
	H_2	40.04	39.81	3.15
	CO_2	24.16	23.32	3.48
	CH_4	10.64	11.27	5.92
400	CO	29.67	27.30	7.98
	H_2	32.99	35.11	6.43
	CO_2	18.4	17.83	3.10
	CH_4	18.93	19.76	7.34
500	CO	31.74	29.31	7.66
	H_2	36.49	39.17	7.34
	CO_2	19.14	18.43	3.71
	CH_4	12.63	13.09	3.64
600	CO	29.51	27.18	7.56
	H_2	38.12	41.13	7.63
	CO_2	19.58	17.86	8.78
	CH_4	12.79	13.83	8.13

The measured gas concentration (vol. %, N_2 free) at different pyrolysis temperature was compared with values obtained from the simulation as shown in Table 11. The results show that the highest gas yield (58 wt. %) was achieved at the highest pyrolysis temperature of 600°C and the least value (23 wt. %) was obtained at 300°C. For the char yield, the highest fraction of char (46 wt. %) was obtained at 300°C, while the least amount of char fraction (~21 wt. %) was observed at 600°C. The high yield of char means a very low conversion of wood sawdust to volatile products; hence the least gas yields occurring at the lowest pyrolysis temperature of 300°C and vice versa.

Table 11 shows the gas concentrations in the non-condensed gas products from the pyrolysis-steam reforming of the wood sawdust. The model considers CO, H_2, CO_2, and CH_4 as the main gas components. The effects of the C_2-C_4 hydrocarbons were lumped into the CH_4 fraction for simplicity. As shown in Table 11, the highest H_2 concentration (41 vol. %) and the lowest CO concentration (27 vol. %) were obtained at pyrolysis temperature of 600°C. The simulation results matched reasonably well with the experimental results.

5 Process Analysis

5.1 Product yields

Figure 5, Figure 6, and Figure 7 shows the comparison of the product yields (gas, bio-oil and char) from the pyrolysis of wood sawdust at increasing temperature. The char yield (Figure 5)

shows a rapid decrease with time. This trend is similar for the different pyrolysis temperature. The char yield decreases with increase in pyrolysis temperature from 300ºC – 600ºC with individual steady state value approached at nearly 10 seconds after the start of the pyrolysis reaction. The actual time taken to achieve complete conversion in the reactor is dependent on the heating rate applied and the ultimate analysis of the biomass sample.
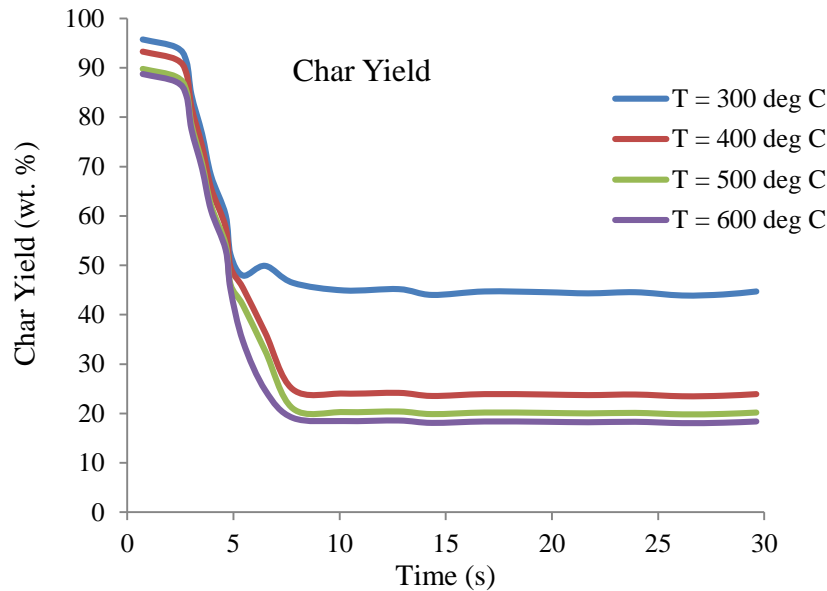

Figure 5 Char yield at different pyrolysis temperature

The oil and the gas yield (Figure 6 and Figure 7) show a similar trend at different pyrolysis temperature. The steady state value approached at nearly 10 seconds after the start of the pyrolysis reaction. The time taken to achieve steady oil yield from each biomass is dependent on the heating rate applied and the ultimate analysis of the biomass samples.
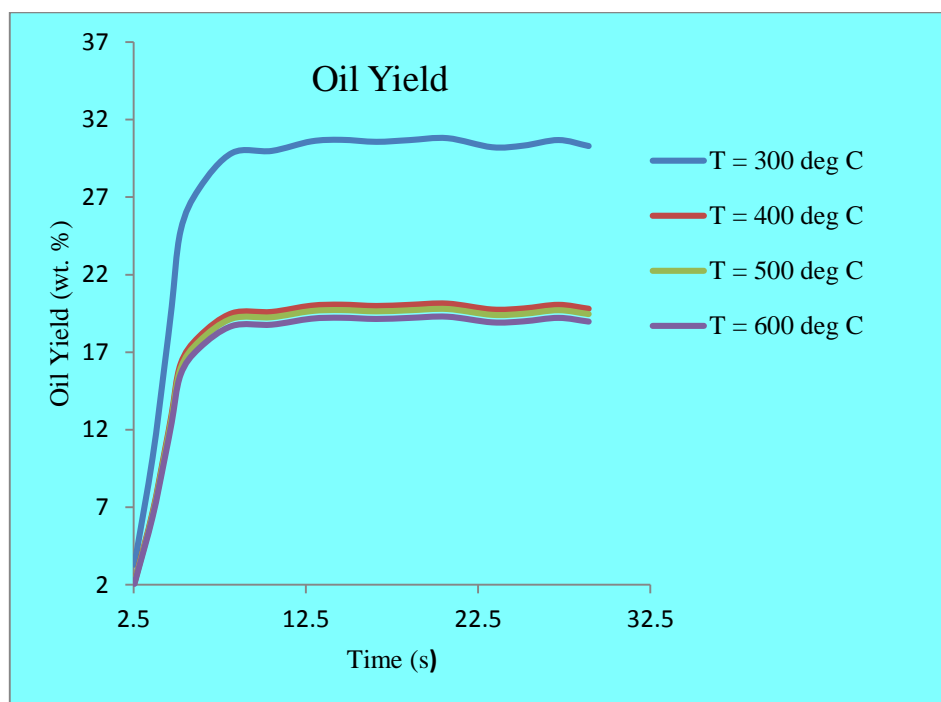

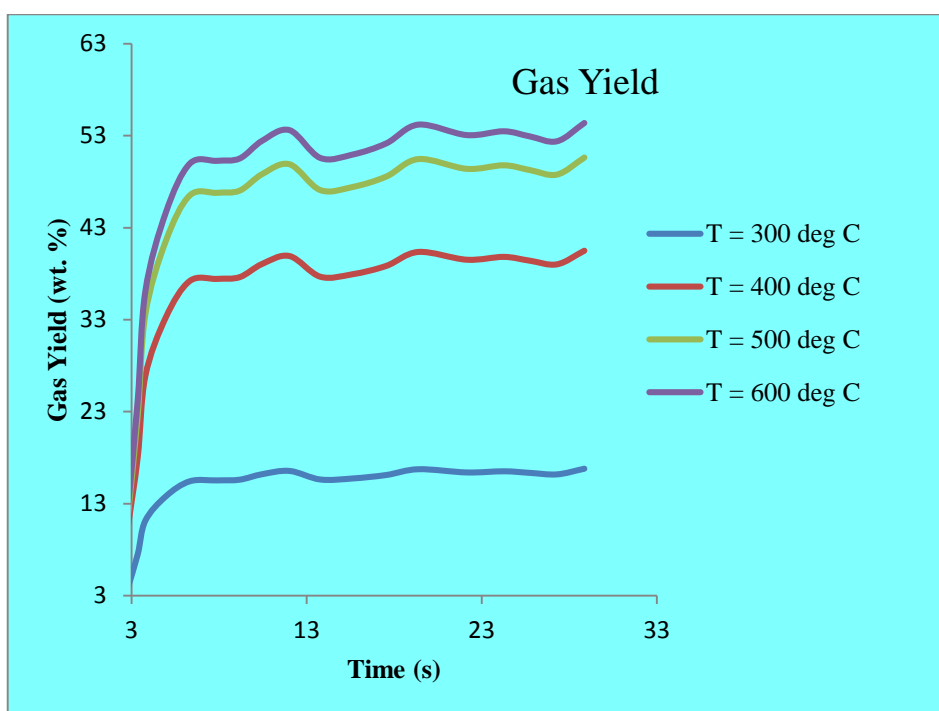Figure 6 Oil yield at different pyrolysis temperature

Figure 7 Gas yield at different pyrolysis temperature

5.2   Gas Concentration

Figure 8 shows the gas concentrations (vol. %) as a function of increasing pyrolysis temperature. It shows that the increase of reaction temperature favours the hydrogen production as H_2 concentration increases from 35% to 41%. On the contrary, CO shows a decrease from 30% to 26%. CH_4 decreases slightly from 20% to 13% and CO_2 decreases from 24% to 14%. This indicates that the temperature plays an important role in the gas concentration and the hydrogen yield.

5.3   Hydrogen Yield

The yield of H_2 (in mmol/g biomass sample) from the model is shown in Table 11. The yield of H_2 increases from 4 to 11 mmol/g at increasing pyrolysis temperature (300°C - 600°C) as shown in Table 10. The H_2 produced may be due to the influence of the catalyst particle model described in section 3.5. The influence of the type of catalyst on hydrogen production was investigated by Wu et al, 2013. The predicted H_2 yield is in good agreement with the experimental results.
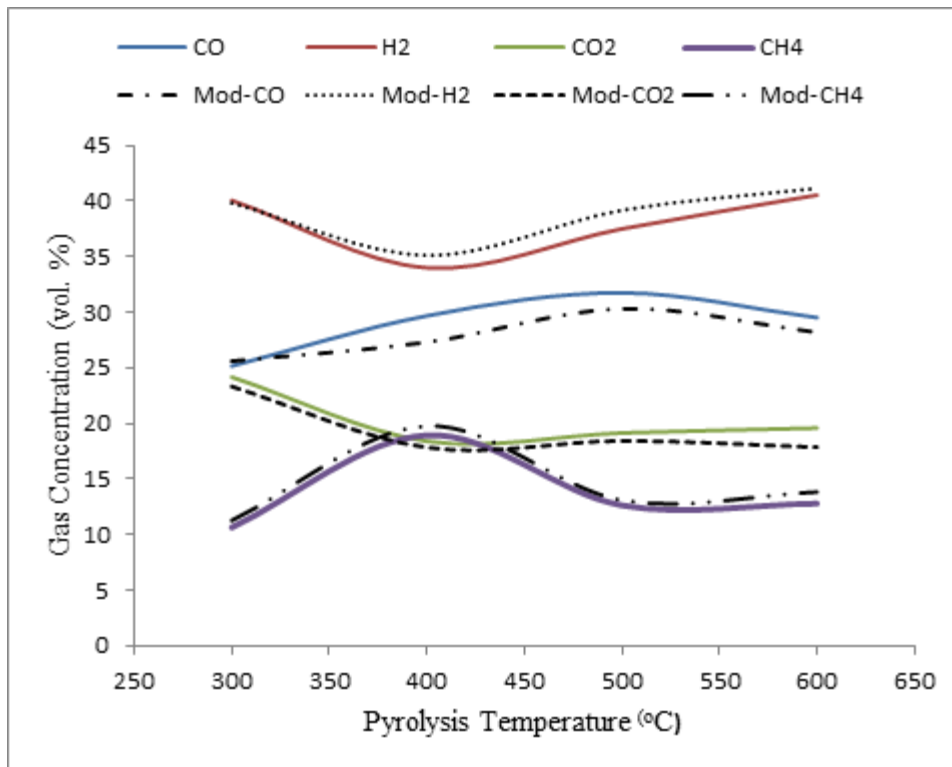
Figure 8 Gas Concentration (vol. %) at increasing pyrolysis temperature

5.4   Temperature Profile in the fixed bed reactors

The temperature at any point in the reactor at any time can be determined from the model. Figure 9 and Figure 10 show the temperature profile in the first and second stage fixed bed reactor respectively from the gPROMS® model. The first reactor was initially heated to the pyrolysis temperature (i.e. 300ºC, 400ºC, 500ºC, and 600ºC). Similarly, the second reactor was initially heated to a temperature of 800ºC, before the volatiles and non-condensable gases from the first-stage reactor were introduced. The fluid phase temperature profile in the second-stage reactor is shown in Figure 9 and Figure 10. Figure 9 shows the change in temperature along the reactor length within 1 to 5 seconds (at a time step of 0.01s) after the start of the reaction and Figure 10 shows the profile after 5 to 30s of simulation. As can be seen from the profile, the temperature increase along the reactor length (z = 0 m to z = 2m). The fluid temperature profile oscillates within 500ºC to 800ºC at the beginning of the reforming process (Figure 9) to a more moderate once (Figure 10) as the reforming reaction progresses.
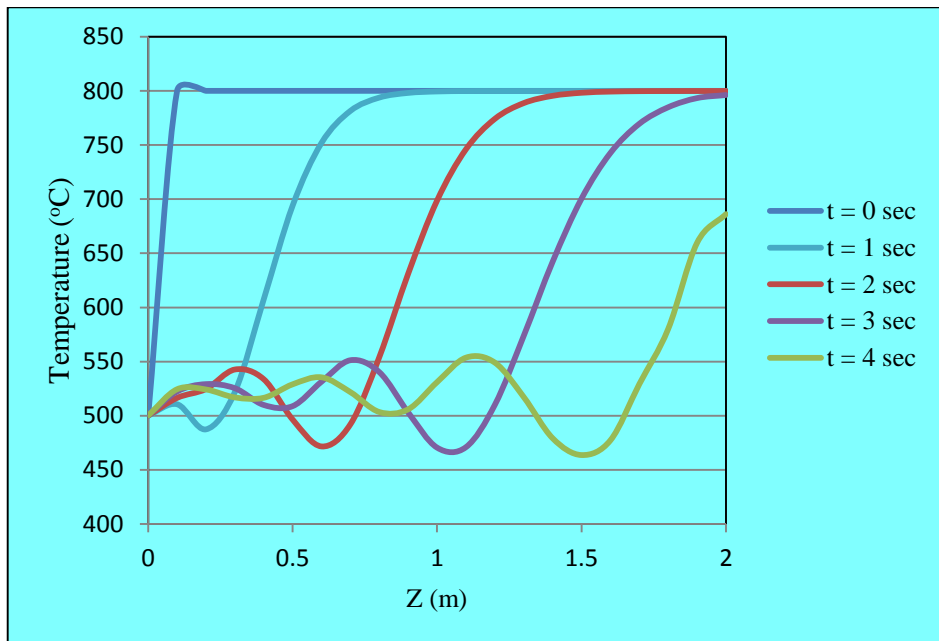
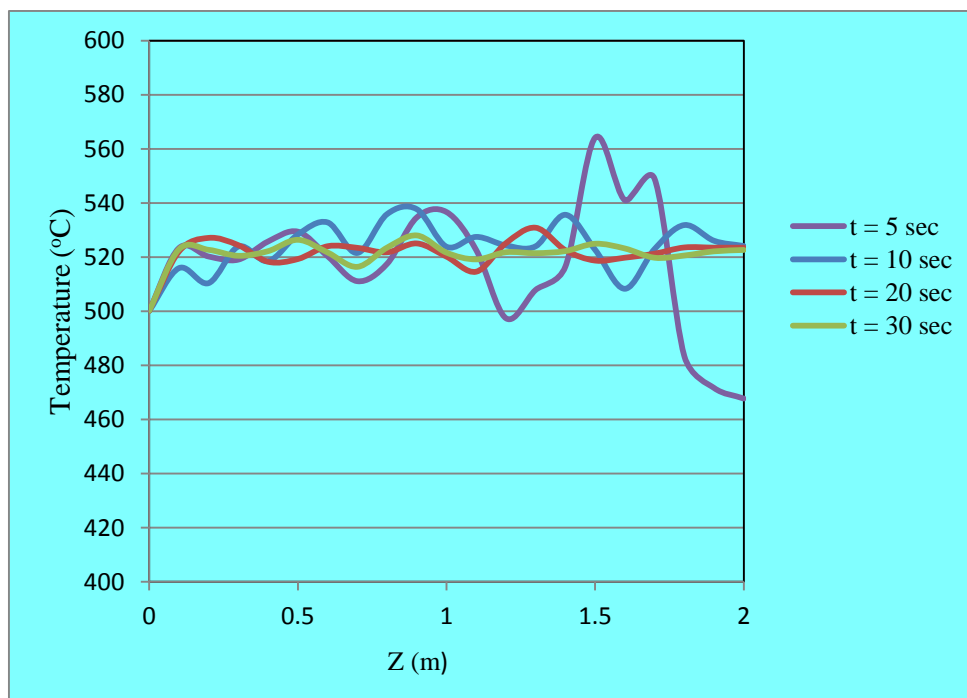Figure 9: Temperature Profile in the fixed bed reactor

Figure 10: Temperature Profile in the fixed bed reactor

6 Conclusion and Recommendation for Future Work

Hydrogen has been identified as a clean and renewable source expected to play a significant role in the future energy systems. This paper presents new experimental results for pyrolysis under different temperatures and development of a dynamic model of biomass pyrolysis/steam reforming of wood sawdust in two-stage fixed bed reactors. The model was validated with experimental data. The model shows good agreement with the experimental

data in predicting the product yields from pyrolysis, hydrogen yield and the temperature profile in steam reforming stage. The dynamic model can be used to predict the hydrogen production capability of different biomass feedstock (i.e. wood, grass, rice husk etc.). In the future, such a model can be improved to predict product yields of biomass pyrolysis/steam gasification based on the mass fraction of the biomass' main components (i.e. cellulose, hemicellulose and lignin). The influence of different catalyst particle in the process can also be included.

References

[1]   Wu, C., Wang, L., Williams P.T., Shi, J., Huang, J., (2011). Hydrogen production from biomass gasification with Ni/MCM-41 catalyst: Influence of Ni content. *Appl. Catalysis B: Environ.* 108-109, 6-13.

[2]   Chen, G., Zhao, L. (2012), Preliminary investigation on hydrogen-rich gas production by co-steam-reforming of biomass and crude glycerin. Int. J. Hydrogen Energy 37; 765–73.

[3]   Wu, C., Williams P.T., (2009), Hydrogen production by steam gasification of polypropylene with various nickel catalysts. *Appl. Catalysis B: Environ* 2009; 87:152–61.

[4]   Tinaut, F.V., Melgar, A., Perez, J.F., Horrillo, A. (2008). Effect of biomass particle size and air superficial velocity on the gasification process in a downdraft fixed bed gasifier. An experimental and modelling study. Fuel Proc. Tech. 89, 1076-1089.

[5]   Inayat, A., Ahmad, M.M., Mutalib, M.I., Yunus, M.K., (2009). Kinetic Modeling of Biomass Steam Gasification System for Hydrogen Production with CO2 Adsorption, Proceedings of Int. Conf. Tech. Pos. (TECHPOS 2009), Kula Lumpur, Malaysia, 14-15 December, 2009.

[6]   Elumalai, S., Pan, X. J. (2011). Chemistry and Reactions of Forest Biomass in Bio-refining, Biological Systems Engineering, University of Wisconsin−Madison, 460 Henry Mall, Madison, WI 53706.

[7]   Wampler T., (2006). *Applied Pyrolysis handbook*. CRC Press Taylor & Francis Group, ISBN-13: 978-1-57444-641 Page 1-6.

[8]   Di Blasi, C., (1997), Influences of physical properties on biomass devolatilization characteristics, Fuel 76 (10), 957-964.

[9]   Di Blasi, (2004), *Modeling Wood Gasification in a Countercurrent Fixed-Bed Reactor,* American Institute of Chemical Engineers AIChE J, 50: 2306–2319, 2004.

[10]   Wu, C., Wang, Z., Dupont, V., Huang, J., Williams, P.T., (2013b). *Nickel-catalyzed pyrolysis /gasification of biomass components*. J. Anal. Appl. Pyrolysis 99, 143-148.

[11]   Luo, Z., Wang, S., Cen, K., (2005), A model of wood flash pyrolysis in fluidized bed reactor. Renewable Energy 30, 377-392.

[12]   Efika, C., Wu C., Williams P.T., (2012). Syngas production from pyrolysis-catalytic steam reforming of waste biomass in a continuous screw kiln reactor. J. Anal. Appl. Pyrolysis 95, 87-94.

[13]   Ghavipour, M., Behbahani, R.M., (2013). Fixed bed reactor modelling for methanol to dimethyl ether (DME) reaction over y-Alumina using a new practical reaction rate model. J. Ind. Eng. Chem. In Press (2013).

[14]   Hashimoto K., Hasegawa, I., Hayashi, J., Mae, K., (2011). Correlations of kinetic parameters in biomass pyrolysis with solid residue yield and lignin content, Fuel 90, 104–112.

[15]   Bamford, C. H., Crank, J., Malan, D.H., (1946). The combustion of wood. Part I. *Mathematical Proc. Camb. Phil. Soc.,* 42(2), 166-182.

[16] Bilbao R., Mastral, J.F., Ceamanos, J., Aldea, M.E. (1996). Modelling of pyrolysis of wet wood. *J. Anal. Appl. Pyrolysis,* 36, 81-97.

[17] Matsumoto T., Fujiwara T., Kondo J., (1969). 12th Symposium on Combustion, The Combustion Institute, Pitts : 515-531.

[18] Koufopanos, C., Papayannakos, N., Maschio, G. & Lucchesi, A. (1991). Modelling of the pyrolysis of biomass particles. Study on kinetics, thermal and heat transfer effects. Canadian Journal of Chemical Engineering, 69, 907-15.

[19] Di Blasi C., (2008). Modelling chemical and physical processes of wood and biomass pyrolysis. Prog. Energy. Combust. Sci. 34, 47-90.

[20] Wu C., Wang Z., Huang J., Williams P. T., (2013a) Pyrolysis/gasification of cellulose, hemicellulose and lignin for hydrogen production in the presence of various nickel-based catalysts. *Fuel*, 106; 697-706.

[21] Chan W. C. R., (1983), Analysis of chemical and physical processes during pyrolysis of large biomass pellets, PhD thesis, Dept. Chem. Eng., University of Washington.

[22] Sinha, S., Jhalani, A., Ravi, M.R., Ray, A. (2000) Modelling of pyrolysis in wood: a review. J. Solar Energy Soc. India 10, 41–62.

[23] Boronson M.L., (1987), *Secondary Reactions of Tars from Pyrolysis of Sweet Gum Hardwood*, PhD thesis, Dept. Chem. Eng., M. I. T., United States.

[24] Wu, C., Wang, L., Williams P.T., Shi, J., Huang, J., (2011). Hydrogen production from biomass gasification with Ni/MCM-41 catalyst: Influence of Ni content. *Appl. Catalysis B: Environ*. 108-109, 6-13.

[25] Byden, K.M., and Ragland, K., (1996). Numerical Modelling of a Deep, Fixed-Bed Combustor, Energy and Fuels, 10, 269.

[26] Corella, J., Aznar, M.P., Delgado, J., Aldea, E., (1991). Steam Gasification of Cellulosic Wastes in a Fluidized Bed with Downstream Vessels, Industrial Engineering Chemistry Research, 30, 2252.

[27] Rioche, C., Kulkarni, S., Meunier F.C., Breen, J.P., Burch, R., (2005). Steam reforming of model compounds and fast pyrolysis of bio-oil on supported noble metal catalysts, App. Catalysis B: Env. 61, 130-139.

[28] Akande, A., Aboudheir, A., Idem, R., Dalai A., (2006). Kinetic modelling of hydrogen production by the catalytic reforming of crude ethanol over a co-precipitated Ni-Al$_2$O$_3$ catalyst in a packed bed tubular reactor, *Int. J. Hydrogen Energy*, 31, 1707-1715.

[29] Ranz, W.E. and Marshall, W.R. Jr., (1952). Evaporation from Drops, Chem. Eng. Prog. 48, Part I, 141-146; Part II, 173-180.

[30] Muske, K.R., Rawlings, J.B., 1995. Nonlinear moving horizon state estimation. In: Berber, R. (Ed.), Methods of Model Based Process Control. Kluwer Academic Publisher, Netherlands.